THE JOURNAL OF PHYSICAL CHEMISTRY B

Article

pubs.acs.org/JPCB

Surfactant-Free Microemulsion Composed of Oleic Acid, *n*-Propanol, and H_2O

Jie Xu,[†] Aolin Yin,[†] Jikuan Zhao,[†] Dongxiang Li,[†] and Wanguo Hou*[,†,‡]

[†]State Key Laboratory Base of Eco-chemical Engineering, Qingdao University of Science and Technology, Qingdao 266042, People's Republic of China

[‡]Key Laboratory for Colloid and Interface Chemistry of Education Ministry, Shandong University, Jinan 250100, People's Republic of China

Supporting Information

ABSTRACT: Generally, a microemulsion consists of oil, water, surfactant, and sometimes cosurfactant. Herein, we report a surfactant-free microemulsion (denoted as SFME), consisting of oleic acid (oil phase), water, and *n*-propanol without the amphiphilic molecular structure of a traditional surfactant. The phase behavior of the ternary system was investigated, showing that there were a single-phase microemulsion region and a multiphase region in the ternary phase diagram. The electrical conductivity measurement was employed to investigate the microregions of the single-phase microemulsion region, and three different microregions, that is, water-in-oleic acid (W/O), a bicontinuous (B.C.) region, and oleic acid-in-water (O/W), were identified, which were further confirmed by freeze-fracture and cryogenic transmission electron microscopy (FF-TEM and Cryo-TEM) observations. The polarity and the salt solubility of water domains in the W/O SFME were investigated by UV−visible spectroscopy using methyl orange and potassium ferricyanide as probes, respectively. Experimental results showed that the water domains in the W/O microemulsion had a lower polarity than bulk water and a normal solubility for salt species, indicating that the SFMEs have much significance in the preparation of various nanomaterials.

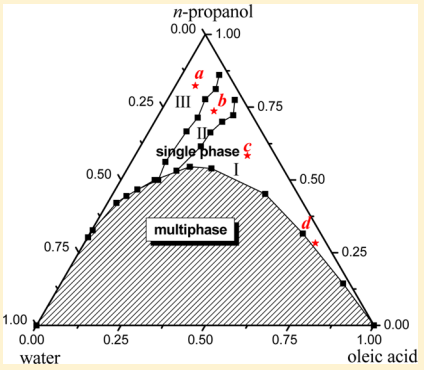

INTRODUCTION

Microemulsion is an optically isotropic, transparent, and thermodynamically stable medium formed by two or more immiscible liquids that are stabilized by an adsorbed surfactant film at the liquid−liquid interface.[1] In the past decades, microemulsions have been an interesting subject because they have been successfully applied to many fields, such as separation,[2] chemical reactions,[3−5] nanomaterial preparations,[6,7] and drug delivery.[8]

Typically, a microemulsion consists of oil, water, and amphiphile,[9] and it is believed that the amphiphile or surfactant is the necessary component in stabilizing the system. However, Smith et al.[10] in 1977 reported an oil-continuous (or water-in-oil, W/O) microemulsion composed of hexane, 2-propanol, and water, and this ternary system could be considered as a surfactant-free (or detergentless) microemulsion (denoted as SFME) because no traditional surfactant was involved in the system. Subsequently, the SFMEs have attracted much attention,[11−19] and it was found that the phase and tension behavior of the systems were similar to those observed with a surfactant-based microemulsion. Herein, we report a ternary system composed of oleic acid, water, and *n*-propanol that can be considered as a surfactant-free microemulsion because *n*-propanol does not have a traditional amphiphilic molecular structure and shows very low surface activity for both oleic acid and water.

Generally, the surfactant-based microemulsions can show different microstructures, namely, oil-in-water (O/W), a bicontinuous (B.C.) structure, and water-in-oil (W/O).[20−23] To get a better insight into SFMEs, it is necessary to investigate their microstructures and structural transitions, which can be identified by various methods, for example, conductivity measurement,[24−26] diffusion coefficient,[27−29] and cyclic voltammetry.[30,31] Conductivity is the most frequently used simple technique to investigate microstructures and structural changes on the basis of the percolation theory. The static percolation model has been proposed to describe the mechanism of percolation in a surfactant-based microemulsion, which attributes percolation to the appearance of a bicontinuous water structure. It is assumed in this description that the open water channel is responsible for electrical conduction.[20,32] The sharp increase of the electrical conductivity in a W/O microemulsion can be explained by a connected water path in the system. In addition, a dynamic percolation model was also developed based on the attractive interactions between the water droplets or micelles.[20] From this point of view, the interactions between water globules are responsible for the formation of percolation clusters and the charge transport is

Received: October 17, 2012
Revised: December 4, 2012
Published: December 11, 2012

assured by hopping of ions on globule clusters that rearrange in time. Electrical conductivity has been studied extensively in recent years and is also used for some new types of microemulsions.[33,34]

To our knowledge, microemulsions have been widely used in the preparation and processing of various materials.[35−37] In the production of metal or semiconductor nanomaterials, water-in-oil microemulsions are employed as aqueous microreactors. The solubility and chemical reactivity of a solute are dependent on the micropolarity of dispersed droplets in microemulsions. To extend SFMEs to the field of nanomaterials, it is necessary to investigate the micropolarity of dispersed droplets and the solubilization of metal salts. Methyl orange and potassium ferricyanide have been frequently used as probes to detect the microenvironment polarity and metal salt solubility in many reverse microemulsions.[33,38−41]

In this paper, the microstructures and the structure transitions of the SFME composed of oleic acid, *n*-propanol, and water were investigated by electrical conductivity, and three different microregions, water-in-oleic acid (W/O), bicontinuous (B.C.), and oleic acid-in-water (O/W) regions, were identified, which were further proved by freeze-fracture and cryogenic transmission electron microscopy (FF-TEM and Cryo-TEM) observations. The polarity and the salt solubility of water domains in the W/O SFME were characterized with methyl orange and potassium ferricyanide as probes, respectively.

EXPERIMENTAL SECTION

Materials. All chemicals used were of normal laboratory reagent grade. Oleic acid and *n*-propanol were purchased from Tianjin Chemical Reagents Co., and methyl orange from Beijing Chemical Reagent Co., and potassium ferricyanide from Shanghai Experimental Reagent Co. Triple-distilled water was used throughout this study. The conductivity of oleic acid, *n*-propanol, and water are 0, 0.161, and 0.577 $\mu S \cdot cm^{-1}$, respectively.

Procedures and Apparatus. The phase behavior of the system was determined by the direct observation method. Mixtures of oleic acid and water with varying volume ratios of oleic acid to water ($R_{o/w}$) from 0.5:9.5 to 9.5:0.5 were prepared in a series of dry test tubes. The samples were placed in a thermostatted water bath at 25.0 ± 0.2 °C and kept well covered to prevent any loss due to evaporation with constant stirring. *n*-Propanol was dropwise added to the mixtures, and kept more than 10 min; the *n*-propanol volumes causing the mixtures to become clear were noted to determine the phase boundaries. The entire procedure was repeated three times, and an average value (the relative deviation was less than ±0.2%) was used to plot the phase diagram.

A low-frequency (50 Hz) conductivity meter (DDS-12DW, Shanghai Lida Precision Instrument Co., Ltd.) with an accuracy of ±1% was used to measure the conductivity of the microemulsion at 25.0 ± 0.2 °C.

Freeze-fracture and cryogenic transmission electron microscopy (FF-TEM and Cryo-TEM) observations were performed, respectively, to study the microstructures of the microemulsion. Fracturing and replication were carried out in a high-vacuum freeze-etching system (BAF-400D, Balzers AG, Liechtenstein). The fracture surface was replicated by shadowing with Pt-C. The metal replicas were viewed in the transmission electron microscopy (TECNAI20, FEI Co.). Cryo-TEM samples were prepared in a controlled environment vitrification system (CEVS) at 25 °C.[42] A micropipet was used to load 5 μL of microemulsion onto a TEM copper grid, which was blotted with two pieces of filter paper, resulting in the formation of thin films suspended on the mesh holes. After waiting for about 5 s, the samples were quickly plunged into a reservoir of liquid ethane (cooled by the nitrogen) at −165 °C. The vitrified samples were then stored in the liquid nitrogen until they were transferred to a cryogenic sample holder (Gatan 626) and examined with a JEOL JEM-1400 TEM (120 kV) at about −174 °C. The phase contrast was enhanced by underfocus. The images were recorded on a Gatan multiscan CCD and processed with Digital Micrograph.

Small-angle X-ray scattering (SAXS) experiments were carried out on an HMBG-SAX small-angle X-ray system (Austria) with Ni-filtered Cu Kα radiation (0.154 nm) operating at 50 kV and 40 mA. Dynamic light-scattering (DLS) experiments were carried out on Dawn Heleos, Wyatt QELS, and Optilab DSP instruments (Wyatt Technology Co., Santa Barbara, CA). Zeta potentials of samples were measured by a zeta potential analyzer (Malvern ZS90, Malvern Instruments Ltd., Worcestershire, U.K.) and a folded capillary cell.

The UV−vis spectra were performed on a computer-controlled UV−vis spectrometer (TU-1901, Beijing Purkinje General Instrument Co. Ltd., China). The path length of the quartz cell used in this experiment was 1 cm. Appropriate amounts of substances were uniformly mixed in advance and then added to the quartz cell. The experiments were carried out at 25 ± 0.2 °C.

All the solutions used for measurements were filtered through a 0.45 μm Millipore Durapore filter.

RESULTS AND DISCUSSION

Phase Behavior of Oleic Acid/*n*-Propanol/Water System. The ternary phase diagram of the oleic acid/*n*-propanol/water system at 25 ± 0.2 °C is shown in Figure 1, in which the component content in the system is in volume fraction. A single isotropic region extending from oil-rich to

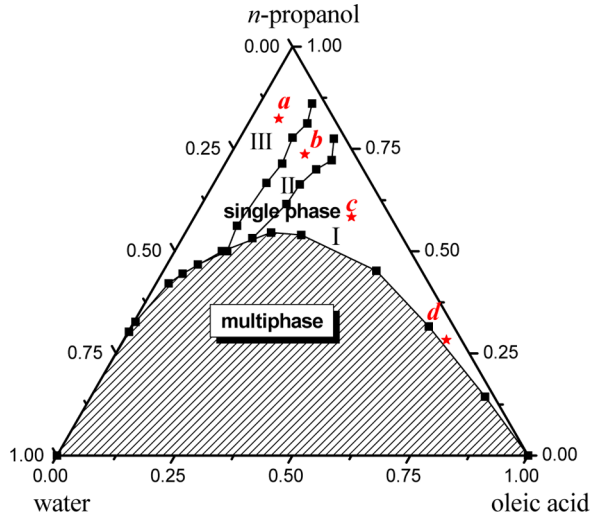

Figure 1. Phase diagram of the oleic acid/*n*-propanol/water three-component system at 25 ± 0.2 °C. The component content in the system is in volume fraction. I, II, and III represent water-in-oleic acid (W/O), bicontinuous (B.C.), and oleic acid-in-water (O/W) regions, respectively. Samples *a*, *b*, *c*, and *d* are chosen for FF-TEM and Cryo-TEM observations and SAXS and DLS measurements.

dx.doi.org/10.1021/jp310282a | J. Phys. Chem. B 2013, 117, 450−456

water-rich regions can be observed. The blank region marked "single phase" is the one-phase microemulsion, and the shadow region marked "multiphase" is a multiphase region, that is, a microemulsion in equilibrium with an excessive water or oleic acid phase.

Generally, the W/O microemulsions can be formed at low water content and the oil is a continuous phase. With increasing water content progressively, as long as there is no phase separation and the system remains isotropic, there should be some kind of gradual structural transition in surfactant-based aqueous microemulsions. The transition should span the range of possible structures from microdroplets to bicontinuous structures. Similarly, for the current SFMEs, the single-phase channels are suitable for the study of the microstructures and structural transitions.[33,43]

Electrical Conductivity Measurements and Microregions of the Oleic Acid/*n*-Propanol/Water Microemulsion. For surfactant-based aqueous microemulsions, Clausse et al.[44] demonstrated that, with increasing water content, the microemulsion electrical conductivity (k) has different changes according to four successive stages: (1) the initial nonlinear increase of k reveals the existence of a percolation phenomenon that may be attributed to the inverse microdroplet aggregation; (2) the next linear increase is due to the formation of aqueous microdomains that results from the partial fusion of clustered inverse microdroplets and suggests that a W/O microemulsion is formed in the low water content region; (3) the third nonlinear curve increase indicates that the medium undergoes further structural transitions and forms a bicontinuous microstructure that is ascribed to the progressive growth and interconnection of the aqueous microdomains; and (4) the final decrease of k corresponds to the appearance of water-continuous microemulsion-type media. That is, an O/W microemulsion forms at high water content, and the progressive decrease of k is ascribed to the progressive decrease of the concentration of the O/W microemulsion droplets.

However, when we determined the conductivity of the three-component system using water as the titration phase at a given volume ratio of *n*-propanol to oleic acid ($R_{p/o}$), it was found that the conductivity curve with increasing water volume fraction (f_w) was progressively increased until the system became turbid (Figure S1, Supporting Information). This indicates that no structural transition occurred with the increase of f_w value. In this case, we have attempted to identify the structural transitions of the oleic acid/*n*-propanol/water microemulsion by using insulative oleic acid as the titration phase, as similarly reported in the literature.[34,41]

Figure 2 shows the variations of electrical conductivity with respect to the oleic acid volume fraction (f_o) at different volume ratios of water to *n*-propanol ($R_{w/p}$). It can be seen that, with increasing f_o value, the k value initially increases and then decreases; at a constant f_o value, the k value increases monotonically with $R_{w/p}$. In addition, the k value of the three-component system is much higher than that of pure water. As a comparison, the k values of the binary solutions of water/*n*-propanol and oleic acid/*n*-propanol were determined, respectively, and the results showed that they were lower than that of pure water (Figure S2, Supporting Information). The higher k values of the three-component system can be attributed to the existence of charged microdroplets, indicating the formation of a microemulsion.[45]

For clarity, the plots of k versus f_o at $R_{w/p}$ = 1:7 and 1:4.33 are shown in Figure 3. According to the opinion of Clausse et al.[44] and refs 34 and 41, the microstructures of the system can be identified based on the plots of k versus f_o. With increasing f_o, the initial increase of k, due to the successive increase of conductive O/W microemulsion droplets, could indicate the formation of an O/W microemulsion; the next nonlinear decrease revealed that the medium underwent a structural transition and became bicontinuous, owing to the progressive growth and interconnection of the O/W microdomains. The third section of the curve, a linear decrease of k, could be interpreted as the consequence of the formation of the W/O

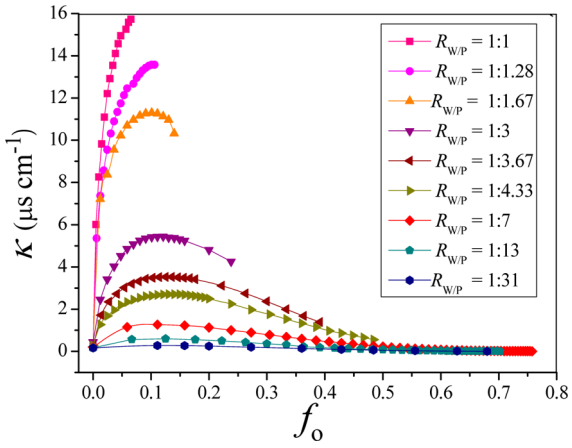

Figure 2. Conductivity k of the microemulsion as a function of f_o at different $R_{w/p}$ values.

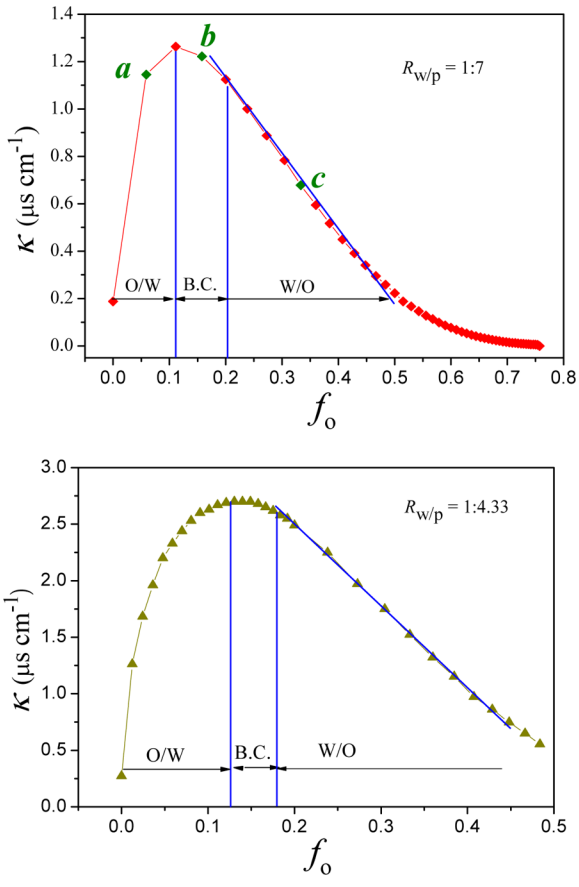

Figure 3. Electric conductivity k of the microemulsion as a function of f_o at $R_{w/p}$ = 1:7 and 1:4.33, respectively. Samples *a*, *b*, and *c* on the $R_{w/p}$ = 1:7 line are chosen for FF-TEM and Cryo-TEM observations.

dx.doi.org/10.1021/jp310282a | J. Phys. Chem. B 2013, 117, 450−456

microdomain resulting from the partial fusion of clustered inverse microdroplets; the final nonlinear decrease of k with further increasing the oil content corresponded to the existence of a percolation phenomenon that could be ascribed to inverse microdroplet aggregation. The conductivity curves in Figure 3 evidently illustrate the presence of three different types of microstructures, that is, O/W, bicontinuous (B.C.), and W/O microemulsions. By repeating the experiment for other samples with different $R_{w/p}$ values (see Figure 2), three types of microregions can be determined, and the subregions identified are also marked in Figure 1.

To explore the origin of the charges on the microdroplets, the pH values of the three-component system as a function of f_w and f_o were first determined (Figures S3 and S4, Surpporting Information), and the results show that the pH values of the microemulsions are less than 5. Therefore, it can be concluded that the change of k could not be attributed to the pH change. This is because the pK_a of oleic acid is around 9.0; the lower pH value (less than 5) of the microemulsion means that the dissociation of oleic acid to oleate can be negligible.[46] Second, the zeta potential of the oleic acid-in-water dispersion prepared by a sonication method was measured, and it was found that the oil microdroplets were negatively charged and the zeta potential was as high as −33.7 mV. A similar result was reported in the literature.[45,47,48] In addition, the zeta potential of the hexane-in-water dispersion was examined, and it was found that the oil microdroplets were negatively charged also and the zeta potential was as high as −30.3 mV. These results imply that hydroxyl ions can be preferentially adsorbed at oil/water interfaces.[45,47,48] Therefore, we believe that the charges of the microemulsion droplets arise from the accumulation of OH^- anions at the oil/water surface. However, the reason for the preferential adsorption of OH^- anions is not clear now.

In addition, it can be seen from the ternary phase diagram containing subregions (Figure 1) why the k value increases progressively with f_w at a constant $R_{p/o}$. This is because the water dilution routes used for k measuring are located completely in a same type of subregion (Figure S1, Supporting Information), which shows that the three-component system studied is not suitable for identifying the structural transitions by using water as the titration phase.

Freeze-Fracture and Cryogenic Transmission Electron Microscopy Observations. To examine the presence of three different types of microstructures, FF-TEM and Cryo-TEM observations were performed for three selected samples with the volume ratios of water/*n*-propanol/oleic acid ($R_{w/p/o}$) at 2:14:1, 2:14:3, and 1:7:4 (as marked by *a*, *b*, and *c* in Figure1), which represent the O/W, the bicontinuous, and the W/O microregions, respectively. Figure 4 shows the FF-TEM and Cryo-TEM images of these samples. From the FF-TEM micrograph, the spherical droplets (white circles in Figure 4) can be clearly observed for sample *a* in the O/W microregion and sample *c* in the W/O microregion. The diameter of the O/W and W/O microemulsion droplets is about 40 and 15 nm, respectively. However, no droplets can be observed for sample *b* in the bicontinuous microregion while a network-like structure can be found; this is because both water and oil are continuous phases.[49]

These morphologies are confirmed by the Cryo-TEM images. That is, the spherical droplets can be observed for samples *a* and *c*, whereas a network-like structure can be found for sample *b*. In addition, the micrograph of sample *a* in the O/W microregion obviously differs from that of sample *c* in the W/O microregion. The sparsely dispersed globular particles (black circles in Figure 4) of sample *a* are darker, whereas the densely packed droplets (arrowheads in Figure 4) of sample *c* are lighter gray than the background. This phenomenon is similar to the published results.[50] All of these results verify the three microregions of the microemulsion, that is, O/W, bicontinuous, and W/O microregions.

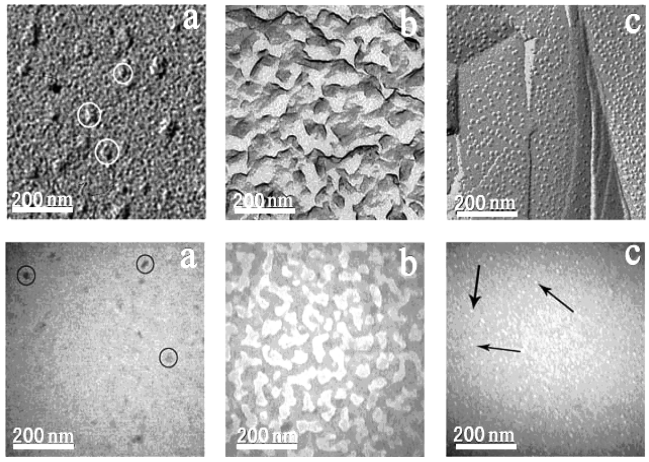

Figure 4. FF-TEM (top) and Cryo-TEM (bottom) images of the selected samples with $R_{w/p}$ = 1:7 and f_o of (a) 0.059 in the O/W microregion, (b) 0.158 in the bicontinuous microregion, and (c) 0.333 in the W/O microregion.

SAXS and DLS Studies. The SAXS technique is a useful technique to provide the information on the microstructure of the microemulsion. The Guinier approximation was often used to obtain the size of the reverse micelles or microemulsions.[51,52] For dilute systems, the apparent gyration radius (R_g) and radius (r) of the micellar core can be obtained by using the Guinier approximation law, which is valid at the low q region and can be expressed as follows[52−55]

$$\ln[I(q)] = \ln[I(0)] - \frac{(qR_g)^2}{3} \quad (1)$$

$$r = (3/5)^{1/2} R_g \quad (2)$$

where q is a scattering vector given in terms of the scattering angle θ by $q = (4\pi/\lambda)\sin\theta$, and $I(0)$ denotes the scattering intensity extrapolated to zero angle.

Figure 5 shows the SAXS curves and Guinier plots for the selected two samples with $R_{w/p/o}$ = 1:7:4 and 1:7:17 (as marked by *c* and *d* in Figure 1). As can be seen, in a small q range of 0.17−0.32 nm^{-1}, the Guinier plots of $\ln I(q)$ versus q^2 show fairly straight lines, indicating the validity of using the Guinier approximation law in this small angle region. The R_g values of samples *c* and *d* are 5.73 and 5.63 nm, respectively, and their radius (r) values are 7.39 and 7.26 nm, respectively. These agree reasonably with the droplet size obtained from TEM observations.

The sizes and size distribution of the droplets of samples *a*, *c*, and *d* (see Figure 1) were also characterized by the DLS technique (Figure S5, Supporting Information), and their radius values are 39.37, 5.43, and 2.56 nm, respectively, indicating the existence of droplets in the samples.

Microenvironment of the W/O Microemulsion. The local environment within a microemulsion droplet may be characterized by UV−vis measurements with solvatochromic

dx.doi.org/10.1021/jp310282a | J. Phys. Chem. B 2013, 117, 450−456

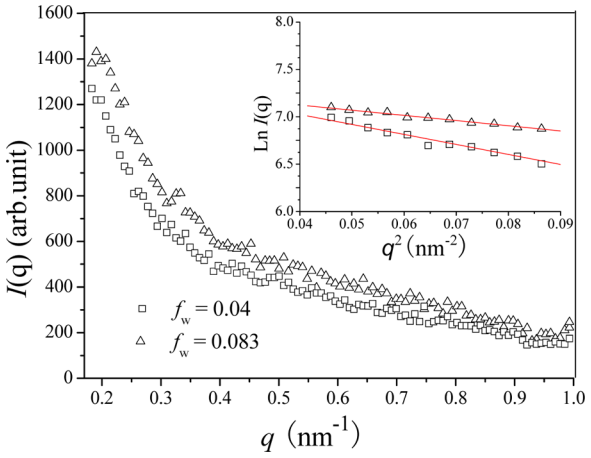

Figure 5. SAXS curves of reverse microemulsion samples *c* and *d* as marked in Figure 1, and the inset shows the corresponding Guinier plots.

probes. The solvatochromic probe selected should be anchored to the polar core of the aggregates, to satisfy the procedural requirement of being soluble in the local environment media. Furthermore, this probe must be sensitive to the polarity of its environment and reflect the polarity through a shift of the absorption maximum. Methyl orange (MO) is a sensitive solvatochromic probe that has been successfully used to detect the microenvironment in many reverse microemulsions.[38−41] As the water content in microemulsions increases, the visible absorption maximum λ_{max} of methyl orange shifts to longer wavelengths (red shift), indicating greater polarity.[39,52] Figure 6

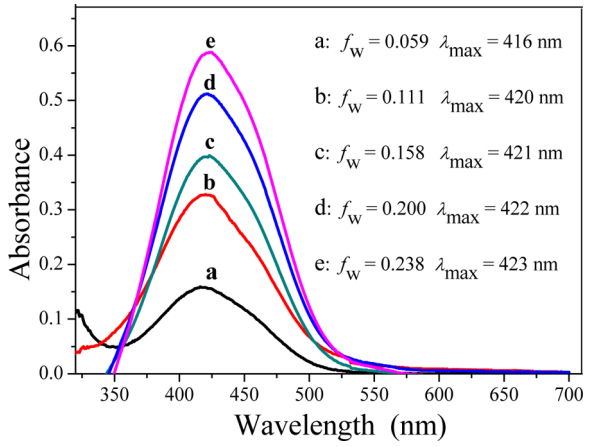

Figure 6. Absorbance of methyl orange in the W/O microemulsion with $R_{p/o}$ = 3:1 as a function of f_w. The MO concentration is 0.096 mmol·L^{-1}.

shows the UV−vis absorbance spectra as a function of different amounts of 0.096 mmol·L^{-1} aqueous methyl orange solution, f_w, in the reverse microemulsion with $R_{p/o}$ = 3:1. As expected, the λ_{max} value of methyl orange increases in the range of 416−423 nm. The λ_{max} of methyl orange is 462 nm in pure water and 415 nm in *n*-propanol. These results suggest that the polarity of the microenvironment of the solubilized methyl orange is intermediate between that of bulk water and *n*-propanol, so the polarity of the water domains in the water-in-oleic acid reverse microemulsion is lower than that of bulk water, which is similar to the published results.[39,52]

Solubility of Salt in the W/O Microemulsion. The use of conventional water-in-oil reverse microemulsions as microreactors is well-established.[18,56] Several different processes have been investigated, including enzymatic reactions and synthesis of metallic and semiconductor nanomaterials. One of the interests in this study is to investigate the possibility of dissolution of ionic metal compounds in SFMEs. These compounds can only dissolve if the solvating properties of the medium approach those of pure water. $K_3Fe(CN)_6$ was chosen mainly due to the fact that $K_3Fe(CN)_6$ is insoluble in the mixture of oleic acid and *n*-propanol, even after prolonged ultrasonication of the mixture. However, after adding water, the microemulsion system takes on a distinct yellow-green color, indicating that $K_3Fe(CN)_6$ is solubilized in microaqueous regions. The UV−vis spectra (Figure 7) reveal that the

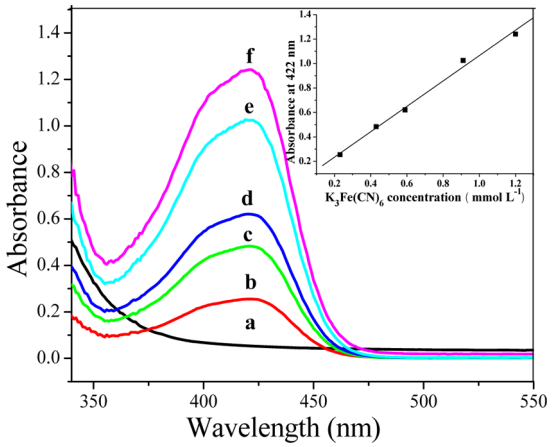

Figure 7. Absorption spectra of $K_3Fe(CN)_6$ in the W/O microemulsion with $R_{w/p/o}$ = 3:14:4 at different $K_3Fe(CN)_6$ concentrations: (a) reference, 0 mmol·L^{-1}; (b) 0.23 mmol·L^{-1}; (c) 0.43 mmol·L^{-1}; (d) 0.59 mmol·L^{-1}; (e) 0.91 mmol·L^{-1}; and (f) 1.20 mmol·L^{-1}. The inset shows the variation of absorbance intensity with $K_3Fe(CN)_6$ concentration.

spectroscopic features are similar to those in conventional aqueous solution. The effect of $K_3Fe(CN)_6$ concentration in the W/O microemulsion on the absorption spectra was also studied. A series of aqueous $K_3Fe(CN)_6$/*n*-propanol/oleic acid microemulsions were prepared with a fixed water, *n*-propanol, and oleic acid volume ratio (3:14:4), but with different $K_3Fe(CN)_6$ concentrations. The observed absorbance of $K_3Fe(CN)_6$ at the maximum wavelength increases linearly with $K_3Fe(CN)_6$ concentration, which is in good agreement with the Lambert−Beer law, as shown by the inset of Figure7.[57] These results confirm the normal solubility of $K_3Fe(CN)_6$ in the SFME studied, similar to the surfactant-based W/O microemulsions.[33,40,41] Considering that $K_3Fe(CN)_6$ is a highly ionic compound and requires a strong aqueous environment to dissolve,[58] the microemulsion system could be able to dissolve other metal ions. Therefore, the SFMEs herein should have potential applications for preparing various nanomaterials or conducting interfacial reactions. One of the advantages of the SFMEs used in nanomaterials as microreactors is to avoid the use of surfactants.

CONCLUSIONS

The phase diagram of the ternary system composed of oleic acid (oil phase), water, and *n*-propanol was determined and

dx.doi.org/10.1021/jp310282a | J. Phys. Chem. B 2013, 117, 450−456

showed a single-phase microemulsion region and a multiphase region. The obtained microemulsion is considered as a surfactant-free microemulsion (SFME). Particularly, the single-phase microemulsion region was successfully identified into three different microregions, that is, water-in-oleic acid (W/O), bicontinuous (B.C.), and oleic acid-in-water (O/W), according to the electrical conductivity measurements, which were further confirmed by FF-TEM and Cryo-TEM observations. The water domains in the W/O microemulsion had a lower polarity than bulk water and a normal solubility for salt species, implying a significant potential of the SFMEs in the preparation of nanomaterials.

■ ASSOCIATED CONTENT

Supporting Information

Phase diagram of the oleic acid/*n*-propanol/water three-component system containing subregions and water dilution routes used for electric conductivity (k) measuring and the k values of the microemulsion as a function of f_w under various $R_{p/o}$ conditions (Figure S1). The k values of the binary solutions of water/*n*-propanol and oleic acid/*n*-propanol (Figure S2). The k and pH values of the microemulsion as a function of f_w and f_o (Figures S3 and S4). Size and size distribution of the reverse microemulsions of the oleic acid/*n*-propanol/water system measured by dynamic light scattering (Figure S5). This material is available free of charge via the Internet at http://pubs.acs.org.

■ AUTHOR INFORMATION

Corresponding Author

*E-mail: wghou@sdu.edu.cn. Telephone: +86-0531-88364750. Fax: +86-0531-88364750.

Notes

The authors declare no competing financial interest.

■ ACKNOWLEDGMENTS

This work was supported by the Natural Science Foundation of Shandong Province of China (Nos. 2009ZRB01722 and ZR2009BM043), the National Natural Science Foundation of China (Nos. 20953003 and 20903059), and the Taishan Scholar Foundation of Shandong Province of China (No. ts20070713).

■ REFERENCES

(1) Mehnert, C. P.; Cook, R. A.; Dispenziere, N. C.; Afeworki, M. *J. Am. Chem. Soc.* **2002**, *124*, 12932−12933.
(2) Zhang, R.; Liu, J.; Han, B. X.; He, J.; Liu, Z. M.; Zhang, J. L. *Langmuir* **2003**, *19*, 8611−8614.
(3) Spiro, M.; de Jesus, D. M. *Langmuir* **2000**, *16*, 2464−2468.
(4) Gao, Y. A.; Li, Z. H.; Du, J. M.; Han, B. X.; Li, G. Z.; Hou, W. G.; Shen, D.; Zheng, L. Q.; Zhang, G. Y. *Chem.—Eur. J.* **2005**, *11*, 5875−5880.
(5) Seth, D.; Chakraborty, A.; Setua, P.; Sarkar, N. *Langmuir* **2006**, *22*, 7768−7775.
(6) Summers, M.; Eastoe, J.; Davis, S. *Langmuir* **2002**, *18*, 5023−5026.
(7) He, Y.; Li, Z.; Simone, P.; Lodge, T. P. *J. Am. Chem. Soc.* **2006**, *128*, 2745−2750.
(8) Patrascu, C.; Gauffre, F.; Nallet, F.; Bordes, R.; Oberdisse, J.; de Lauth-Viguerie, N.; Mingotaud, C. *ChemPhysChem* **2006**, *7*, 99−101.
(9) Danielsson, I.; Lindman, B. *Colloids Surf.* **1981**, *3*, 391−392.
(10) Smith, G. D.; Donelan, C. E.; Barden, R. E. *J. Colloid Interface Sci.* **1977**, *60*, 488−496.
(11) Kelser, B. A.; Varie, D.; Barden, R. E.; Holt, S. L. *J. Phys. Chem.* **1979**, *83*, 1276−1280.
(12) Borys, N. F.; Holt, S. L.; Barden, R. E. *J. Colloid Interface Sci.* **1979**, *71*, 526−532.
(13) Knickerbocker, B. M.; Pesheck, C. V.; Scrlven, L. E.; Davis, H. T. *J. Phys. Chem.* **1979**, *83*, 1984−1990.
(14) Lund, G.; Holt, S. L. *J. Am. Oil Chem. Soc.* **1980**, *57*, 264−267.
(15) Lara, J.; Perron, G.; Desnoyers, J. E. *J. Phys. Chem.* **1981**, *85*, 1600−1605.
(16) Knickerbocker, B. M.; Pesheck, C. V.; Davies, H. T.; Scriven, L. E. *J. Phys. Chem.* **1982**, *86*, 393−400.
(17) Puig, J. E.; Hemker, D. L.; Guta, A.; Davies, H. T.; Scriven, L. E. *J. Phys. Chem.* **1987**, *91*, 1137−1143.
(18) Khmelnitsky, Y. L.; vanHoek, A.; Veeger, C.; Visser, A. J. W. G. *J. Phys. Chem.* **1989**, *93*, 872−878.
(19) Zoumpanioti, M.; Karali, M.; Xenakis, A.; Stanmatis, H. *Enzyme Microb. Technol.* **2006**, *39*, 531−539.
(20) de Gennes, P. G.; Taupin, C. *J. Phys. Chem.* **1982**, *86*, 2294−2304.
(21) Kaler, E. W.; Bennett, K. E.; Davis, H. T.; Scriven, L. E. *J. Chem. Phys.* **1983**, *79*, 5673−5684.
(22) Mackay, R. A.; Myers, S. A.; Bodalbhai, L.; Brajter-Toth, A. *Anal. Chem.* **1990**, *62*, 1084−1090.
(23) Ceglie, A.; Das, K. P.; Lindman, B. *Colloids Surf.* **1987**, *28*, 29−40.
(24) Clausse, M.; Peyrelasse, J.; Heil, J.; Boned, C.; Lagourette, B. *Nature* **1981**, *293*, 636−638.
(25) Mehta, S. K.; Kaur, G.; Bhasin, K. K. *Colloids Surf., B* **2007**, *60*, 95−104.
(26) Mehta, S. K.; Kaur, G.; Bhasin, K. K. *Pharm. Res.* **2008**, *25*, 227−236.
(27) Lindman, B.; Kamenka, N.; Kathopoulis, T. M.; Brun, B.; Nilsson, P. G. *J. Phys. Chem.* **1980**, *84*, 2485−2490.
(28) Chew, C. H.; Gan, L. M.; Ongand, L. H.; Zhang, K. *Langmuir* **1997**, *13*, 2917−2921.
(29) Johannessen, E.; Walderhaug, H.; Balinov, B. *Langmuir* **2004**, *20*, 336−341.
(30) Mackay, R. A.; Myers, S. A.; Bodalbha, L.; Brajter-Toth, A. *Anal. Chem.* **1990**, *62*, 1084−1090.
(31) Mo, C. S. *Langmuir* **2002**, *18*, 4047−4053.
(32) Ponton, A.; Bose, T. K.; Delbos, G. *J. Chem. Phys.* **1991**, *94*, 6879−6886.
(33) Gao, Y. A.; Li, N.; Zheng, L. Q.; Zhao, X. Y.; Zhang, S. H.; Han, B. X.; Hou, W. G.; Li, G. Z. *Green Chem.* **2006**, *8*, 43−49.
(34) Gao, Y. A.; Wang, S. Q; Zheng, L. Q.; Han, S. B.; Zhang, X.; Lu, D. M.; Yu, L.; Ji, Y. Q.; Zhang, G. Y. *J. Colloid Interface Sci.* **2006**, *301*, 612−616.
(35) Ghosh, H. N.; Adhikari, S. *Langmuir* **2001**, *17*, 4129−4130.
(36) Yin, Z. L.; Sakamoto, Y.; Yu, J. L.; Sun, S. X. *J. Am. Chem. Soc.* **2004**, *126*, 8882−8883.
(37) Khomane, R. B.; Manna, A.; Mandale, A. B.; Kulkarni, B. D. *Langmuir* **2002**, *18*, 8237−8240.
(38) Clarke, M. J.; Harrison, K. L.; Johnston, K. P.; Howdle, S. M. *J. Am. Chem. Soc.* **1997**, *119*, 6399−6406.
(39) Zhu, D. M.; Schelly, Z. A. *Langmuir* **1992**, *8*, 48−50.
(40) Gao, Y. A.; Li, N.; Zheng, L. Q.; Zhao, X. Y.; Zhang, J.; Cao, Q.; Zhao, M. W.; Li, Z.; Zhang, G. Y. *Chem.—Eur. J.* **2007**, *13*, 2661−2670.
(41) Gao, Y. A.; Li, N.; Zhang, S. H.; Zheng, L. Q.; Li, X. W.; Dong, B.; Yu, L. *J. Phys. Chem. B* **2009**, *113*, 1389−1395.
(42) Liu, C. C.; Hao, J. C. *J. Phys. Chem. B* **2011**, *115*, 980−989.
(43) Gao, Y. A.; Han, S. B.; Han, B. X.; Li, G. Z.; Shen, D.; Li, Z. H.; Du, J. M.; Hou, W. G.; Zhang, G. Y. *Langmuir* **2005**, *21*, 5681−5684.
(44) Clausse, M.; Zradba, A.; Nicolas-Morgantini, L. *Microemulsions Systems*; Dekker: New York, 1987.
(45) Franks, G. V.; Djerdjev, A. M.; Beattie, J. K. *Langmuir* **2005**, *21*, 8670−8674.
(46) Kamogawa, K.; Okudaira, G.; Matsumoto, M.; Sakai, T.; Sakai, H.; Abe, M. *Langmuir* **2004**, *20*, 2043−2047.

(47) Beattie, J. K.; Djerdjev, A. M. *Angew. Chem., Int. Ed.* **2004**, *43*, 3568−3571.
(48) Marinova, K. G.; Alargova, R. G.; Denkov, N. D.; Velev, O. D.; Petsev, D. N.; Ivanov, I. B.; Borwankar, R. P. *Langmuir* **1996**, *12*, 2045−2051.
(49) Hoffmann, H.; Thunig, C.; Munkert, U.; Meyer, H. W.; Richter, W. *Langmuir* **1992**, *8*, 2629−2638.
(50) Wolf, L.; Hoffmann, H.; Talmon, Y.; Teshigawarac, T.; Watanabe, K. *Soft Matter* **2010**, *6*, 5367−5374.
(51) Hirai, M.; Kawai-Hirai, R.; Yabuki, S.; Takizawa, T.; Hirai, T.; Kobayashi, K.; Amemiya, Y.; Oya, M. *J. Phys. Chem.* **1995**, *99*, 6652−6660.
(52) Liu, J. C.; Han, B. X.; Zhang, J. L.; Li, G. Z.; Zhang, X. G.; Wang, J.; Dong, B. Z. *Chem.—Eur. J.* **2002**, *8*, 1356−1360.
(53) Eastoe, J.; Paul, A.; Nave, S.; Steytler, D. C.; Robinson, B. H.; Rumsey, E.; Thorpe, M.; Heenan, R. K. *J. Am. Chem. Soc.* **2001**, *123*, 988−989.
(54) Maitra, A. *J. Phys. Chem.* **1984**, *88*, 5122−5125.
(55) Li, J. C.; Zhang, J. L.; Gao, H. X.; Han, B. X.; Gao, L. *Colloid Polym. Sci.* **2005**, *283*, 1371−1375.
(56) Hu, G.; O'Hare, D. *J. Am. Chem. Soc.* **2005**, *127*, 17808−17813.
(57) Meziani, M. J.; Sun, Y. P. *Langmuir* **2002**, *18*, 3787−3791.
(58) Hutton, B. H.; Perera, J. M.; Grieser, F.; Stevens, G. W. *Colloids Surf., A* **2001**, *189*, 177−181.